

METAL ORGANIC FRAMEWORKS DERIVED NICKEL SULFIDE/GRAPHENE  
COMPOSITE FOR LITHIUM-SULFUR BATTERIES

A Thesis

Presented to

The Graduate Faculty of University of Akron

In Partial Fulfillment

of the Requirement for the Degree of

Master of Science

Yijie Ji

May 2018

METAL ORGANIC FRAMEWORKS DERIVED NICKEL SULFIDE/GRAPHENE  
COMPOSITE FOR LITHIUM-SULFUR BATTERIES

Yijie Ji

Thesis

Approved

Accepted

---

Advisor  
Dr. Yu Zhu

---

Dean of College  
Dr. Eric J. Amis

---

Faculty Reader  
Dr. Steven S. C. Chuang

---

Dean of the Graduate School  
Dr. Chand K. Midha

---

Department Chair  
Dr. Coleen Pugh

---

Date

## ABSTRACT

With the increasing demanding of energy density and power density in electric vehicles (EVs) and unarmed aerial vehicles, novel rechargeable battery technology with higher performance is required.<sup>1</sup> Lithium-sulfur battery is considered as a promising second battery for replacing lithium ion battery (LIB), due to its high theoretical specific capacity and low cost. However, the stability and coulombic efficiency of current Li-S cells are still not satisfactory for many applications. One of the major issue is the cell degradation due to the shuttle effect of soluble polysulfide (PS).<sup>2</sup> Here in this thesis, we introduce a metal organic frameworks (MOFs) derived NiS/Graphene composite as cathode host material for Li-S battery. MOFs were used as a precursor to prepare carbon framework with well-organized nanostructure.<sup>3</sup> NiS was used to provide good affinity with lithium polysulfide, mitigating shuttle effect. In addition, graphene acted as substrate for anchoring MOFs nanoparticles and provided necessary electron transport passages. The Li-S cell with the designed cathode exhibited improved electrochemical performances. A reversible capacities of 1366 mA h g<sup>-1</sup> at a current density of 0.05 C, 609 mA h g<sup>-1</sup> at a 3 C were achieved (1 C = 1675 mA h g<sup>-1</sup>). In addition, a good stability (98 % capacity retention after 400 cycles) was observed at 0.75 C.

## ACKNOWLEDGEMENT

First of all, I would like to present my appreciation to my advisor, Dr. Yu Zhu, who has given me a lot of help, guidance and constructive suggestions during my two-year-research.

Also, I would like to thank Dr. S. C. Chuang as my committee member to my formal seminar and my thesis reader.

Then, I am very thankful to Dr. Feng Zou, a postdoc in my group, and Xinye Liu, a former master student in my group. They taught me how to conduct experiments and guided my work with patience and enthusiasm.

In addition, I want to thank all my other group members, for their help and advice for my work.

Finally, I am grateful to my parents and friends for their support and care on my life and study during the past two years.

## TABLE OF CONTENTS

	Page
LIST OF FIGURES .....	VII
CHAPTER	
I. INTRODUCTION .....	1
1.1 ORIGIN OF BATTERY TECHNOLOGY AND ITS APPLICATION.....	1
1.2 LITHIUM-SULFUR BATTERY -- A PROMISING ENERGY SYSTEM.....	3
1.3 MECHANISM OF LITHIUM-SULFUR BATTERY .....	4
1.4 CHALLENGES FOR DEVELOPMENT OF LITHIUM-SULFUR BATTERY .....	7
1.5 METAL SULFIDE CATHODE MATERIAL FOR LI-S BATTERY .....	8
1.6 METAL ORGANIC FRAMEWORKS (MOFs) DERIVED NANOSTRUCTURED MATERIAL .....	9
1.7 METAL ORGANIC FRAMEWORKS (MOFs) DERIVED NiS/GRAPHENE COMPOSITE .....	10
II. EXPERIMENTAL SECTION .....	12
2.1 MATERIALS .....	12
2.2 SYNTHESIS OF Ni-MOF/GRAPHENE PRECURSOR .....	12
2.3 SYNTHESIS OF NiS/GRAPHENE COMPOSITE .....	13
2.4 BATTERY FABRICATION.....	13
2.5 CHARACTERIZATION .....	14
2.5.1 Scanning electron microscope (SEM) .....	14
2.5.2 X-ray diffraction (XRD) .....	14
2.5.3 Thermal gravimetric analysis (TGA).....	14

2.5.4 Raman spectroscopy .....	15
2.5.5 Electrochemical performances.....	15
III. RESULTS AND DISCUSSION.....	16
3.1 MORPHOLOGY CHARACTERIZATION FOR Ni-MOF/GRAPHENE PRECURSOR, CARBON- COATED Ni/GRAPHENE COMPOSITE AND NiS/GRAPHENE COMPOSITE .....	16
3.2 CHARACTERIZATION FOR PURITY OF NiS .....	19
3.3 THERMAL ANALYSIS FOR COMPOSITE COMPOSITION .....	20
3.4 CHARACTERIZATION OF GRAPHENE IN THE COMPOSITE .....	21
3.5 LITHIUM POLYSULFIDE ADSORPTION TEST .....	22
3.6 ELECTROCHEMICAL PERFORMANCES .....	24
3.6.1 Cyclic voltammetry (CV) .....	24
3.6.2 Galvanostatic charge/discharge test .....	26
3.6.3 Rate capability .....	27
3.6.4 Long cycle performance .....	28
CONCLUSIONS .....	30
REFERENCES .....	31

## LIST OF FIGURES

Figure	Page
1. (a) Comparison among $\text{LiMO}_2$ , $\text{LiMO}_2/\text{silicon}$ and $\text{Li-S}$ calculated on energy density. <sup>2</sup> (b) Comparison between lithium-sulfur and lithium ion on voltage, capacity and specific energy. <sup>1</sup> .....	4
2. A traditional discharge and charge curve of lithium-sulfur batteries. <sup>13</sup> .....	6
3. Charge/discharge curve with different sulfur-containing species at four parts. (the inset presents mechanism of the polysulfide shuttle effect). <sup>14</sup> .....	6
4. Illustration of the reaction sequence and polysulfide shuttle of $\text{Li-S}$ cell. <sup>167</sup>	
5. Volume expansion of sulfur after lithiation. <sup>17</sup> .....	8
6. Illustration of metal organic framework (MOF). <sup>36</sup> .....	10
7. SEM images of $\text{Ni-MOF/Graphene}$ composite synthesized with different reaction time (a) 2 hours; (b) 6 hours; (c) 10 hours; (d) SEM image under higher resolution at the area in the red region of 10 hours' composite.....	17
8. SEM images of (a) $\text{Ni-MOF/Graphene}$ composite dried by traditional oven. (b) $\text{Ni-MOF/Graphene}$ composite dried by freeze-drying. (c) carbon-coated $\text{Ni/Graphene}$ composite. (d) $\text{NiS/Graphene}$ composite.....	19
9. X-ray diffraction (XRD) pattern of composite after sulfurization, indicating the formation of $\text{NiS}$ .....	19
10. Thermal gravimetric analysis (TGA) of carbon-coated $\text{Ni/Graphene}$	

composite and thiourea mixture. (N <sub>2</sub> ; temperature: raised to 500 °C; ramp-rate: 10 °C min <sup>-1</sup> ).....	21
11. Thermal gravimetric analysis of NiS/Graphene composite. (Air; temperature: raised to 600 °C; raising ramp-rate: 10 °C min <sup>-1</sup> ).....	21
12. Raman spectrum of Ni-MOF/Graphene and NiS/Graphene composite. 22	13.
Lithium polysulfide (Li <sub>2</sub> S <sub>6</sub> ) absorption test. (a) drop a low concentration of Li <sub>2</sub> S <sub>6</sub> solution in Ni-MOF/Graphene precursor and NiS/Graphene composite. (b) change of MOF/Graphene precursor and NiS/Graphene composite after 15 min absorption of Li <sub>2</sub> S <sub>6</sub> . (c) drop a high concentration of Li <sub>2</sub> S <sub>6</sub> solution in Ni-MOF/Graphene precursor and NiS/Graphene composite. (d) change of MOF/Graphene precursor and NiS/Graphene composite after 30 min absorption of Li <sub>2</sub> S <sub>6</sub> . .....	24
14. Cyclic voltammetry (CV) curve of Li-S cell test at voltage window of 1.7- 2.8 V with a scan rate of 0.2 mV s <sup>-1</sup> .....	25
15. Charge/discharge (specific capacity vs. voltage) profile for 1 <sup>st</sup> cycle at current density of 0.15 C (1 C = 1675 mA g <sup>-1</sup> ).....	26
16. Galvanostatic charge/discharge profile (voltage vs. specific capacity) of 1 <sup>st</sup> cycle at current density of 0.05 C, 1 <sup>st</sup> and 100 <sup>th</sup> cycle at 0.15 C, 1 <sup>st</sup> and 400 <sup>th</sup> cycle at 0.75 C.....	27
17. Rate capability of Li-S cells tested at different current density from 0.05 C to 3 C .....	28
18. Long cycle performance (capacity/coulombic efficiency vs. cycle) of Li-S cell tested at 0.75 C. (0.05 C and 0.15 C was used for activation) .....	29

## CHAPTER I

### INTRODUCTION

#### 1.1 Origin of battery technology and its application

In ancient times, the most widely used resources for energy were coal, gas and petroleum. However, these natural resources will eventually run out someday in the future and they cause a lot of damages to our environment like global warming and do harm to the environment. Another problem is that transporting them is inefficient and cost high. These issues are not beneficial to sustainable development. Thus, in the past several decades, people are researching for a new generation of green and rechargeable energy technology, and then came the battery technology. Many kinds of battery technology was researched at that time, such as Li-air battery, Li ion battery, fuel cell and lead-acid battery. Among them, lithium ion batteries (LIBs) was developed since 1980s and is nowadays one of the most mature one.<sup>4</sup>

For a long time, the LIB is considered as a representative energy storage device owing to its high energy density. Also, LIB can last long and is friendly to environment.<sup>5</sup> Up to now, lithium ion battery (LIB) is widely used on cell phones, laptops and many other fields related to our daily life. With the development of battery technology and for the purpose of sustainable development, in recent years, there is increasing demanding for applying battery technology into vehicles to manufacture electric vehicles (EVs). As we all know,

the traditional vehicles run via burning petroleum, which causes a great number of environment problems owing to releasing of carbon dioxide (CO<sub>2</sub>). Thus, using a new generation of green and rechargeable energy technology on vehicles is becoming a trend to reduce vehicles' dependence on petroleum, which leads that many car manufactures and governments are devoted to developing electric vehicles.<sup>6</sup> In early stage of this research, lithium ion battery is the first choice and lithium ion battery can indeed to act as the driving force for vehicles. However, the problem comes that the driving range the electric vehicles could provide after one charge process is not sufficient. The utmost driving range could offer is limited 200 km per charge process. The main cause for this phenomenon is on the mechanism of cathode material for LIB. Typically, lithium ion battery uses transition metal oxide with lithium intercalated like (LiCoO<sub>2</sub>)<sup>7</sup> and (LiFePO<sub>4</sub>)<sup>8</sup>. These materials have intrinsic defect that they can only accept one electron during discharge and charge process owing to only one stable redox state.<sup>1</sup> This limits the energy density of lithium ion battery up to 200 W h kg<sup>-1</sup>. Although lithium ion battery has the advantage of high energy density, it still cannot provide sufficient energy density for application on electric vehicles. Also, other large appliances like unarmed aerials vehicles and satellites, which requires high energy density as well, will also be involved in the application of battery technology in the future.<sup>9</sup> In this way, only using lithium ion battery will limit the development. Therefore, in today's stage, the challenge for developing battery technology is to make the cell could provide with a reliable high energy density. There is another disadvantage for using lithium ion battery: cost. Lithium only occupies 0.0065 wt % on earth, so that cost of producing lithium ion battery is high. These two limitations make lithium ion batteries might not be the best candidate for manufacturing electric vehicles. Thus, researchers keep going on

finding another energy system that can both provide higher energy density and have lower cost. Then they turn their attention to lithium-sulfur batteries.

## 1.2 Lithium-sulfur battery -- A promising energy system

In the past several years, lithium-sulfur batteries is considered a promising candidate and new generation of high energy system to be applied into electric vehicles and many other large electrical appliances that need high energy density.<sup>10</sup> As is discussed above, lithium ion batteries could not provide electric vehicles with sufficient energy density to ensure a long driving range, and the cost is high. However, these two limitations seem to disappear when using lithium-sulfur battery. During discharge process, element sulfur is converted to dilithium sulfide ( $\text{Li}_2\text{S}$ ) by phase transformation, which is different from the intercalation mechanism in lithium ion battery. This comes to the first advantage that lithium-sulfur battery has a theoretical energy density of  $2500 \text{ W h kg}^{-1}$ , which is much higher than traditional LIB of  $200 \text{ W h kg}^{-1}$ .<sup>11</sup> In addition, since sulfur has several stable redox states, the sulfur atom can accept two electrons transferred when transforming from element sulfur to the final product  $\text{Li}_2\text{S}$ . So, the second advantage is that lithium-sulfur battery has a higher theoretical specific capacity of  $1675 \text{ mA h g}^{-1}$ .<sup>12</sup> In Figure 1<sup>1,2</sup>, it can be seen clearly that lithium sulfur batteries could provide a much higher theoretical energy density, specific capacity than lithium ion batteries. In addition, compared with lithium, sulfur has a higher occupation of 2.9 wt % on earth. So its cost is lower. With these three advantages (high energy density, high theoretical capacity and low cost), lithium-sulfur batteries is a good substituent to lithium ion battery applied to electric vehicles.

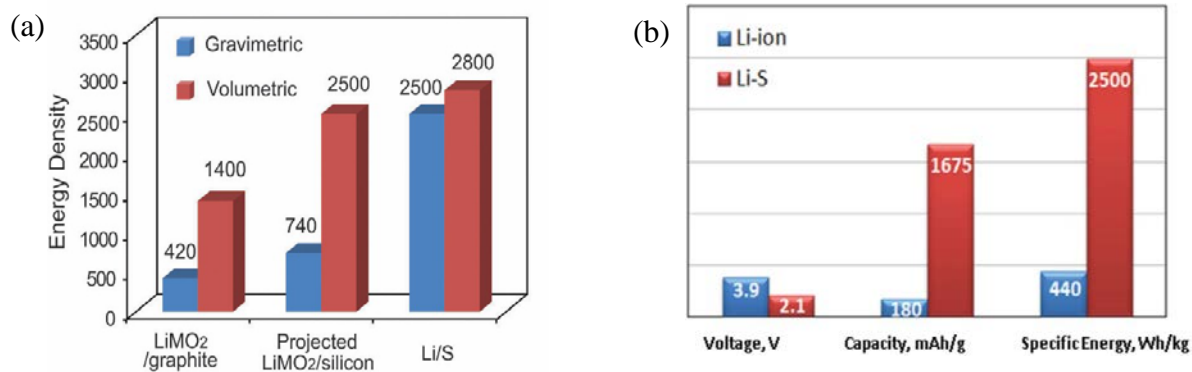
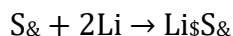


Figure 1. (a) Comparison among LiMO<sub>2</sub>, LiMO<sub>2</sub>/silicon and Li-S calculated on energy density.<sup>2</sup> (b) Comparison between lithium-sulfur and lithium ion on voltage, capacity and specific energy.<sup>1</sup>

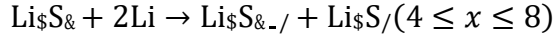
### 1.3 Mechanism of lithium-sulfur battery

Figure 2<sup>13</sup> shows a traditional discharge and charge mechanism of lithium-sulfur batteries. According to the figure, the charge and discharge process can be divided into four parts

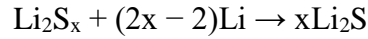
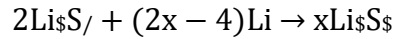
Part 1: During this process happens a reaction between elemental sulfur and element lithium to form long chain lithium polysulfide Li<sub>2</sub>S<sub>8</sub>. This reaction forms the first plateau at 2.2-2.3V during discharge process. Furthermore, Li<sub>2</sub>S<sub>8</sub> is soluble in liquid electrolyte, so that the reaction in this part is a solid to liquid reaction.<sup>13</sup>



Part 2: In this part, the long chain polysulfide formed in part 1 is degraded to short chain polysulfide Li<sub>2</sub>S<sub>x</sub> (4 ≤ x ≤ 8). The chain length of polysulfide ions (PS ion) is reduced. Since the short chain polysulfide is also soluble in the liquid electrolyte, the reaction kinetics between two liquid phases will be rapid and voltage also decreases from this part.<sup>13,14</sup>



Part 3. Here still happens a reduction reaction. The short chain polysulfide is reduced to  $\text{Li}_x\text{S}_x$  or  $\text{Li}_x\text{S}$ . The two competing reactions both make up the second plateau at 1.9-2.1V. As is shown in Figure 2, the second plateau has a long span over capacity, so that this part contributes most to whole capacity in discharge. Also, since  $\text{Li}_x\text{S}_x$  and  $\text{Li}_x\text{S}$  are both in solid state, the reaction kinetics of this part becomes slower than previous part.



Part 4. In this last part,  $\text{Li}_x\text{S}_x$  can be further reduced to  $\text{Li}_x\text{S}$ .  $\text{Li}_x\text{S}$  and  $\text{Li}_x\text{S}_x$  have intrinsic properties of non-conductive and insoluble, so that this process is accompany with high polarization.<sup>13</sup> It can be seen in Figure 2 that voltage decreases a lot in this part because the reaction happens here is a solid state one.



When putting these four parts together, we can get a brief mechanism sequence, which is mostly used nowadays:  $\text{S}_x \rightarrow \text{Li}_x\text{S}_x \rightarrow \text{Li}_x\text{S}_9 \rightarrow \text{Li}_x\text{S}_2 \rightarrow \text{Li}_x\text{S} \rightarrow \text{Li}_x\text{S}_x$ .<sup>15</sup> Figure 3<sup>14</sup> and Figure 4<sup>16</sup> are consistent with the four-part-process. Also, in Figure 3, apart from the reaction sequence, we can see the different kinetics situation for these four parts. The fast to slow reaction kinetics is the same as what is discussed during the four parts above.

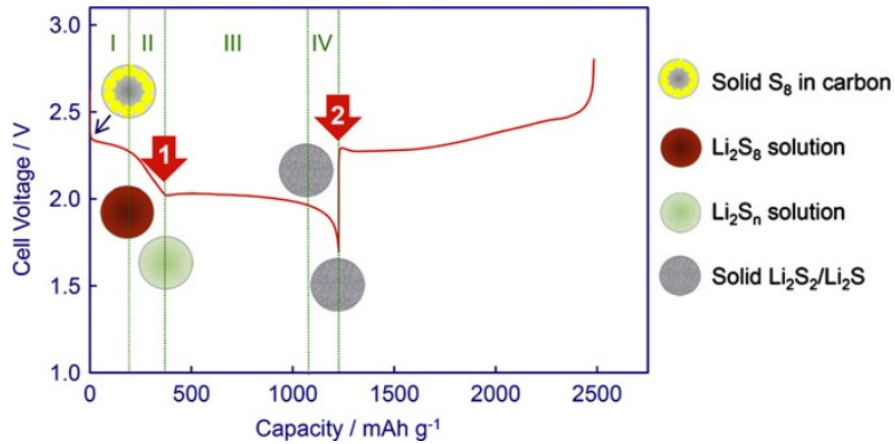


Figure 2. A traditional discharge and charge curve of lithium-sulfur batteries.<sup>13</sup>

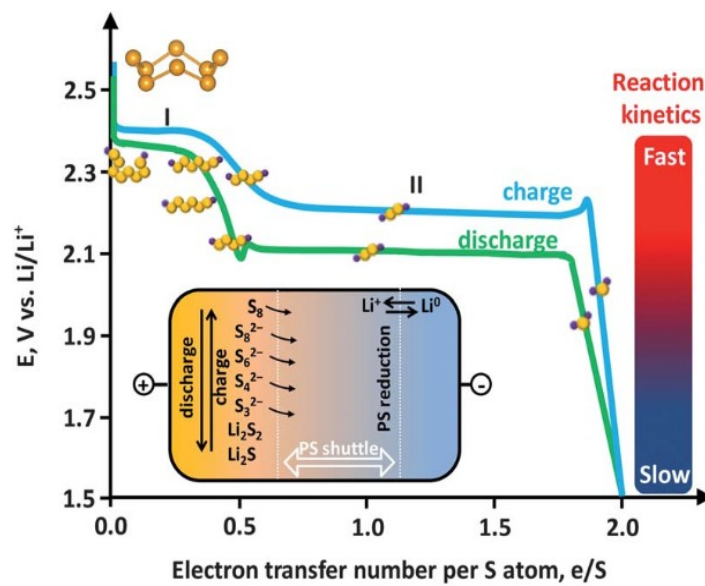


Figure 3. Charge/discharge curve with different sulfur-containing species at four parts.

(the inset presents mechanism of the polysulfide shuttle effect).<sup>14</sup>

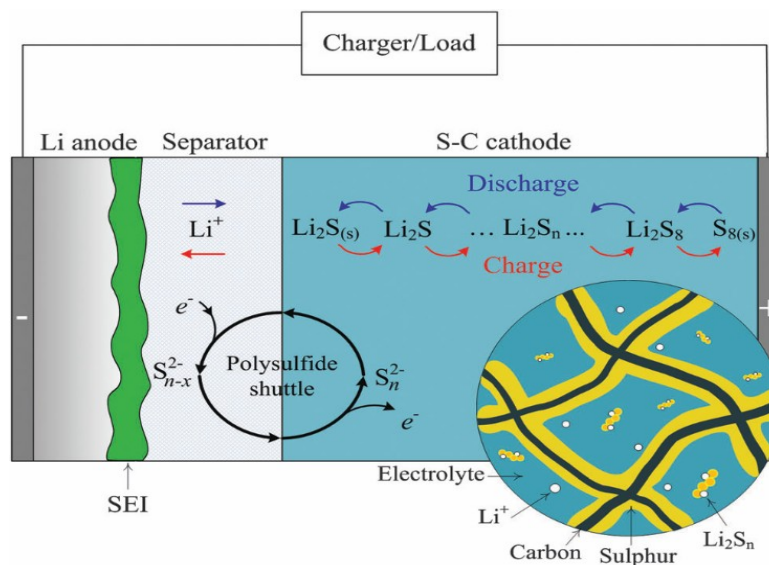


Figure 4. Illustration of the reaction sequence and polysulfide shuttle of Li-S cell.<sup>16</sup>

#### 1.4 Challenges for development of lithium-sulfur battery

Although lithium-sulfur battery has its own advantages over lithium ion battery as mentioned above, there are still some challenges that limits the development and further commercialization. The challenges can be concluded into three parts. First, volume expansion. It is a typical problem in many battery systems. During discharge process, element sulfur reacts with lithium, and after lithiation is completed, the volume of element sulfur will be expanded to 80 % larger.<sup>17</sup> The illustration is shown in Figure 5. When happening the volume expansion, the electrode will be pulverized, leading a loss in capacity. Second, sulfur and final product dilithium sulfide are both insulating and non-conductive. They both have low ion diffusion coefficient and high resistance. When  $\text{Li}_2\text{S}$  is formed at the last two stages of discharge, it will cover on the surface of electrode, which makes the conductivity of whole electrode decrease. Also, further lithiation will be difficult and then

voltage declines a lot in a short time.<sup>2</sup> The third challenge is the most important one in lithium-sulfur battery, which is the soluble lithium polysulfide. The long chain polysulfide can dissolve in liquid electrolyte, moving from cathode to anode. Then, it will be reduced to short chain polysulfide and further reduced to  $\text{Li}_2\text{S}$ , which may form a passive layer on anode. In addition, when the charge process occurs, the short chain polysulfide can also dissolve in electrolyte, diffusing back to cathode and oxidized to the long chain polysulfide again.<sup>18</sup> In brief, the soluble lithium polysulfide can move back and forth between cathode and anode. The phenomenon is so-called shuttle effect. The shuttle effect is illustrated in both insertion part of Figure 3 and Figure 4, and it is the main cause for low stability and low coulombic efficiency of the Li-S cells.

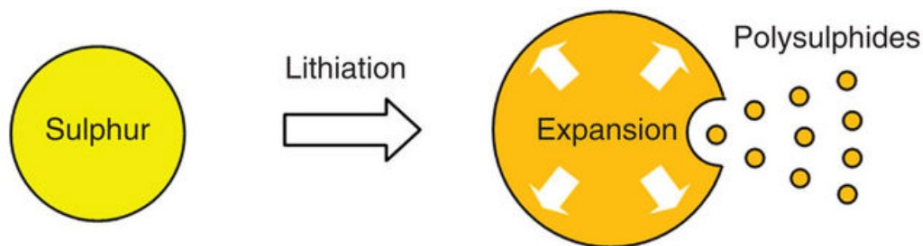


Figure 5. Volume expansion of sulfur after lithiation.<sup>17</sup>

### 1.5 Metal sulfide cathode material for Li-S battery

At early stage, the original cathode composition of lithium-sulfur batteries is element sulfur, carbon black and PVDF as binder. The slurry is casted on the aluminum foil as current collector.<sup>1</sup> However, the problem of the three challenges discussed above exist. Then, attention has been paid to prepared transition metal oxides, sulfides and nitride cathode material like titanium dioxide ( $\text{TiO}_2$ )<sup>19</sup> and vanadium nitride ( $\text{VN}$ )<sup>20</sup>. Among these promising cathode materials, metal sulfides, such as cobalt sulfide ( $\text{Co}_9\text{S}_8$ )<sup>21</sup>, nickel sulfide

(Ni<sub>2</sub>S)<sup>22</sup>, iron sulfide (FeS<sub>2</sub>)<sup>23</sup> and titanium sulfide (TiS<sub>2</sub>)<sup>24</sup> have been highly investigated as cathode material for lithium-sulfur batteries owing to metal sulfide's intrinsic advantages. First, metal sulfides have a strong affinity to sulfur-containing compounds, so that it can be a good absorber and sulfur host to anchor lithium polysulfide to mitigate shuttle effect. Second, overlap happens in the voltage window of lithium-sulfur battery could be relieved owing to low lithiation voltage of metal sulfides.<sup>9</sup> In addition, compared with metal oxides, metal sulfides have higher electrical conductivity, as well as mechanical and thermal stability.<sup>25</sup> These qualities can help to increase capacity and energy density of the cell.

#### 1.6 Metal organic frameworks (MOFs) derived nanostructured material

Only using metal sulfide in electrode is not enough. The structure is another important factor. Bulk electrode will lead to poor electrochemical performance because it has low specific surface area, which results in low capacity and energy density. Then, people began researching on nanostructured electrode material. The nanostructured material has benefits in following ways. First, since the active material is nanostructured, there will be enough space to overcome the volume expansion caused by element sulfur, so that pulverization of electrode can also be avoided.<sup>2</sup> Second, there is more contact room between electrode and electrolyte, which leads to a faster ion diffusion. Also, shorter passages for transporting ions and electrons is provided by nanostructured material.<sup>25,26</sup> Third, with the nanostructure, the final product Li<sub>2</sub>S can deposit on a surface with a much higher specific area compared with bulk material, so that morphology of electrode can be protected from transformation after charge/discharge process.<sup>27-30</sup>

Thus, a nanostructure metal sulfide is needed to overcome the challenges like volume

expansion and shuttle effect, thus further improves electrochemical performances. Metal organic frameworks (MOFs) is widely used as precursor/template for electrode because the nanostructure derived is well-organized, and conductive nanostructured product with carbon coating can be further obtained via thermal annealing the MOF.<sup>3,31,32</sup> MOF consists of metal ions and organic ligands as shown in Figure 6. Both compositions distribute uniformly in structure, so that the nanostructure in the carbon coated product can remain well-organized.<sup>33</sup> For example, sulfur embedded in a nanoporous carbon matrix with nitrogen doping was synthesized derived from ZIF-8 MOF precursor.<sup>34</sup> The MOF derived electrode with stable nanostructure could achieve high electrical conductivity, providing a high energy, power density and also good cycle stability.<sup>35</sup>

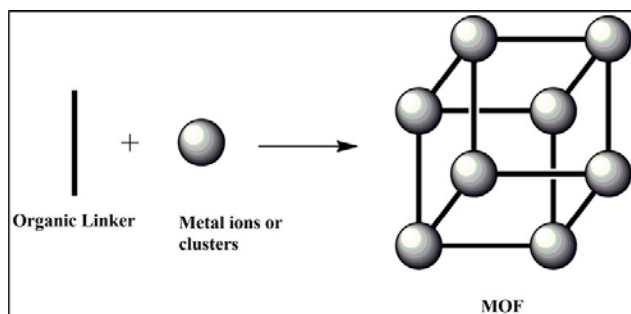


Figure 6. Illustration of metal organic framework (MOF).<sup>36</sup>

### 1.7 Metal organic frameworks (MOFs) derived NiS/Graphene composite

Here in this work, we introduce a metal organic frameworks derived nickel sulfide/Graphene composite. The MOF precursor was synthesized via hydrothermal reaction, in which Ni ions act as the metal cluster and trimesic acid act as the organic ligand. Two further annealing treatments were conducted to obtain the final composite. The first annealing process is also the carbonization process. During this process, the organic ligand

in the MOF precursor was decomposed under a high temperature and form a carbon coating on the Ni ions. The second annealing process is the sulfurization process, in which the Ni ions were converted to NiS by a vulcanizing agent.

Graphene is also used in the composite to form hybrid material with metal sulfide. Although the nanostructure metal sulfide shows advantage, it may still have the problem of aggregation between each other and form a large particle again.<sup>26</sup> Thus, Hybrid materials is then considered as a good choice to prevent the aggregation. Among them, combination of metal sulfide and carbon has been greatly investigated because of its capability to be a sulfur host, providing valid anchor with efficient affinity to lithium polysulfide.<sup>37</sup> In the hybrid material, carbon will act as a buffer to avoid the aggregation of nanoparticles, and at mean time, nanostructured metal sulfide could still release its advantages. Many kind of carbon sources were used before, such as meso/microporous carbon matrix<sup>38</sup>, carbon nanofiber (CNF)<sup>39</sup> and carbon nanotube (CNT)<sup>40</sup>. Here, here we choose the graphene, and graphene oxide (GO) is first used in preparation to be a source to synthesize graphene. Graphene is confirmed to be a good substrate, so that it is used here to anchor Ni-MOF nanoparticles. In addition, compared with other carbon species, graphene has its own advantages such as higher conductivity, higher mechanical flexibility and also higher thermal and chemical stability.<sup>41,42,43</sup>

Thus, the features from metal organic framework, metal sulfide and graphene enable improved electrochemical performances. As is expected, our Li/S cells obtained a reversible capacity of 1366 mA h g<sup>-1</sup> at a current density of 0.05 C (1 C = 1675 mA h g<sup>-1</sup>). In addition, a good stability and coulombic efficiency was obtained at 0.75 C with a perfect retention of 98 % after 400 cycles.

## CHAPTER II

### EXPERIMENTAL SECTION

#### 2.1 Materials

Nickel nitrate hexahydrate ( $\text{Ni}(\text{NO}_3)_2 \cdot 6\text{H}_2\text{O}$ , 99.999%, Sigma-Aldrich), graphene oxide water dispersion (GO, monolayer layer content, 4mg/ml, >95%, polar solvents), trimesic acid (95% Sigma-Aldrich), N, N-dimethylformamide (DMF, ACS grade, EMD), ethanol (200 proof, Decon Laboratories, Inc.), N-methyl-2-pyrrolidone (NMP, 99.5% EMD), lithium bis(trifluoromethanesulfonyl)imide (LiTFSI, Sigma-Aldrich), lithium nitrate ( $\text{LiNO}_3$ , Sigma-Aldrich), 1,3-Dioxolane (DOL, Sigma-Aldrich), 1,2-Dimethoxyethane (DME, TCI), element sulfur (S, 99.5%, Alfa Aesar), carbon black (Super P, Timcal), polyvinylidene fluoride (PVDF,  $M_w = 530\,000\text{ g mol}^{-1}$ , Scientific Polymer Products Inc.), lithium foil (15.6 mm in diameter and 0.25 mm in thickness, MTI cooperation).

#### 2.2 Synthesis of Ni-MOF/Graphene precursor

In a typical synthesis procedure, 324 mg of  $\text{Ni}(\text{NO}_3)_2 \cdot 6\text{H}_2\text{O}$  was dissolved in a mixed solution with 3 ml graphene oxide and 4 ml distilled water under ultrasonic. 112 mg trimesic acid was dissolved in a mixed solution with 7 ml ethanol and 7 ml DMF under ultrasonic. Then, both solutions were mixed together also under ultrasonic. The obtained

black solution was then transferred into a 50 mL Teflon-lined autoclave. The mixture was heated at 150 °C for 10 h in oven after sealing the autoclave. The final product was washed with ethanol and distilled water several times with centrifugation (Eppendorf 5702). Then, the product was dried overnight using freeze-dryer.

### 2.3 Synthesis of NiS/Graphene composite

The as-prepared Ni-MOF/Graphene precursor was heated in a tube furnace to 500 °C with a ramp-rate of 1 °C min<sup>-1</sup>. Argon was filled in the tube to ensure the environment. The subsequent black powder was further heated to 420 °C to do sulfurization of Ni with a ramp-rate of 2 °C min<sup>-1</sup> and isothermal at 420 °C for 2 h. Thiourea was used as vulcanizing agent with a mass ratio of 3:1 to the black powder. Argon was also filled during the process. The NiS/Graphene composite was obtained after the furnace cooling down to room temperature.

### 2.4 Battery fabrication

The as-prepared NiS/Graphene composite was mixed with element sulfur to be the active material at a mass ratio of 3 :7. The active material was then mixed with carbon black and PVDF at a mass ratio of 7 :2 :1. After adding NMP, the mixture was grinded in a mortar to form a homogeneous slurry. Then, the slurry was casted on an aluminum foil current collector by using a doctor blade. After that, the slurry coated foil was dried in an oven at 80 °C overnight and was then cut into 1/2 inches' disk-shape for fabrication of coin cells. The sulfur mass loading was ~ 1 mg cm<sup>2</sup>. The fabrication of the coin cells was accomplished in an Argon filled glovebox. Celgard 3501 was used as separator and disk-

shape lithium foil as counter electrode. Stainless steel and nickel foam were also used. The electrolyte used is 1M LiTFSI in (DOL/DME=1:1 0.1M LiNO<sub>3</sub>) at an amount of 20  $\mu\text{L mg}^{-\text{D}}$  based on the mass of the active material.

## 2.5 Characterization

### 2.5.1 Scanning electron microscope (SEM)

Scanning electron microscope was conducted to investigate morphology of Ni-MOF/Graphene precursor, carbon-coated Ni/Graphene composite and NiS/Graphene composite. The instrument used was JEOF JSM-7401F operating at 10 kV

### 2.5.2 X-ray diffraction (XRD)

X-ray diffraction (XRD) was carried out to analysis the purity, composition and crystallinity of NiS/Graphene composite at the angle range from 0 - 65°. The instrument used was a Rigaku Ultima IV X-ray fiddractorimeter using Cu K<sub>K</sub> radiation ( $\lambda = 1.5604 \text{ \AA}$ ).

### 2.5.3 Thermal gravimetric analysis (TGA)

Thermal gravimetric analysis was conducted to determine sulfurization temperature of carbon-coated Ni/Graphene composite. Sample was heated to 500 °C with a rate of 10 °C min<sup>-1</sup> in N<sub>2</sub>. NiS/Graphene composite was also analyzed to measure NiS and carbon content in the composite. The condition was heating to 600 °C with a rate of 10 °C min<sup>-1</sup> in air. The TGA apparatus was Q500 (TA Instruments).

#### **2.5.4 Raman spectroscopy**

Raman spectroscopy was carried out to characterize graphene in both Ni-MOF/Graphene precursor and NiS/Graphene composite. The instrument used was HORIBA LabRAM HR High-Resolution Raman Microscope.

#### **2.5.5 Electrochemical performances**

The cyclic voltammetry (CV) was measured by using an electrochemical workstation (CHI608E, CH Instrument) at a scan rate of  $0.2 \text{ mV s}^{-1}$ . The galvanostatic discharge/charge tests were performed in a voltage window of 1.7-2.8 V (vs.  $\text{Li/Li}^{\text{Q}}$ ) at different current density of 0.05 C, 0.1 C, 0.15 C, 0.75 C, 1.5 C and 3 C ( $1 \text{ C} = 1675 \text{ mA g}^{-1}$ ). The instrument used was a battery analyzer (MTI BST-8A).

## CHAPTER III

### RESULTS AND DISCUSSION

#### 3.1 Morphology characterization for Ni-MOF/Graphene precursor, carbon-coated Ni/Graphene composite and NiS/Graphene composite

The Ni-MOF precursor was prepared by a hydrothermal reaction. Here we use trimesic acid as the organic ligand/linker and Ni ions as the metal ions/clusters. The Ni-MOF/Graphene precursor was first annealed in an argon filled tube furnace to do carbonization. During this process, the trimesic acid organic ligand was converted to carbon to form carbon-coated Ni-MOF nanoparticles. Then, a further annealing process for sulfurization was conducted. Thiourea was used as vulcanizing agent, converting Ni clusters into the final product nickel sulfide. The Ni-MOF/Graphene composite, carbon-coated Ni-MOF/Graphene composite and NiS/Graphene composite were all characterized with scanning electron microscope (SEM).

Figure 7 (a)-(c) show the SEM images of Ni-MOF/Graphene composite synthesized with different reaction time to observe the development process of morphology. For the 2 hours' composite, the morphology of graphene sheet was unclear, and there were few Ni-MOF nanoparticles in the structure. It was also unclear to see the Ni-MOF particles anchor on the graphene sheet. When came to the 6 hours' composite, there was more graphene sheet and there are more Ni-MOF particles anchor on it. For the final 10 hours' composite,

the morphology of graphene sheet is apparent, and the whole composite was filled with Ni-MOF nanoparticles. Figure 7 (d) shows the part in red square of Figure 7 (c) with a higher resolution, lots of Ni-MOF nanoparticles could be clearly seen anchored on the graphene sheet, which is our expectation. Thus, with reaction time increases, more and more Ni MOF particles anchored on the graphene substrate and morphology of graphene became clear.

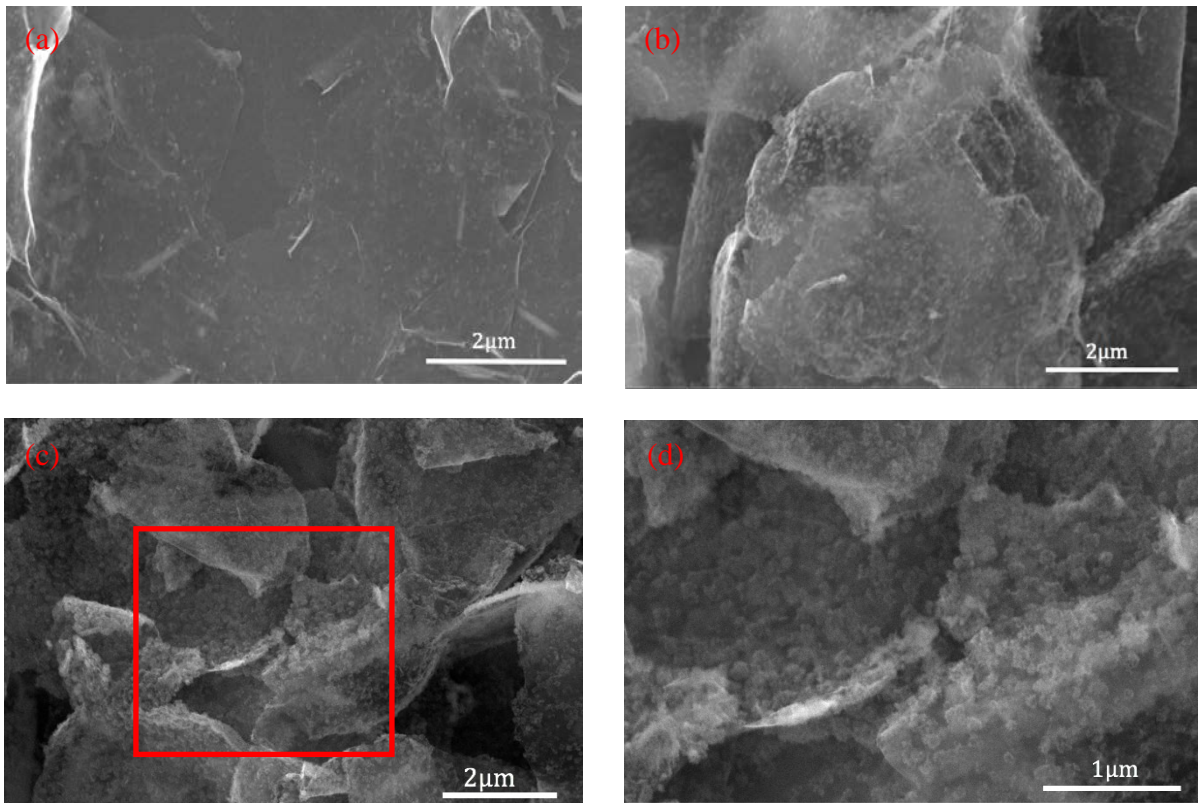


Figure 7. SEM images of Ni-MOF/Graphene composite synthesized with different reaction time (a) 2 hours; (b) 6 hours; (c) 10 hours; (d) SEM image under higher resolution at the area in the red region of 10 hours' composite.

Figure 8 (a) shows the morphology of Ni-MOF/Graphene composite dried by traditional oven. The Ni MOF nanoparticles still anchored on the graphene sheet. However,

the morphology of graphene sheet changed and turned to a hardened substrate, which made the flexibility of graphene disappear. The reason might be that in a traditional oven, the graphene sheets aggregated with each other to form a hardened surface. This pulverized the porous structure of graphene and was unfavorable to further embedding of element sulfur. Nevertheless, when Ni-MOF/ Graphene composite was dried with freeze-drying (Figure. 8b), the morphology of graphene didn't change a lot. It is because that under a low temperature (-40 °C), the aggregation of graphene sheets was avoided and the porous structure was persevered. Figure 8 (c), (d) show the morphology of carbon-coated Ni/Graphene composite and NiS/Graphene composite derived from Ni-MOF/Graphene precursor dried via freeze-drying (Figure. 8b). Although the composite underwent two annealing process to do the carbonization and sulfurization, the morphology remained unchanged. Apart from the morphology was unchanged, there was more and more graphene sheet appeared in the composite after annealing processes.

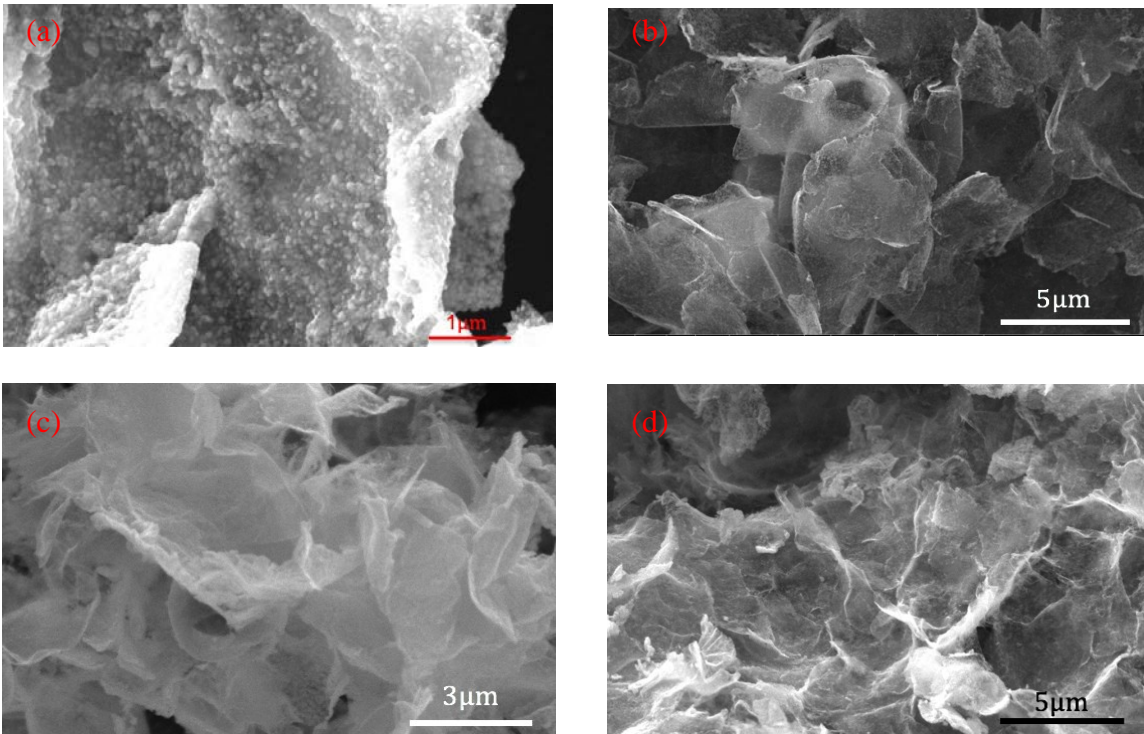


Figure 8. SEM images of (a) Ni-MOF/Graphene composite dried by traditional oven. (b) Ni-MOF/Graphene composite dried by freeze-drying. (c) carbon-coated Ni/Graphene composite. (d) NiS/Graphene composite.

### 3.2 Characterization for purity of NiS

After sulfurization, it is necessary to confirm the successful converting from nickel ion to nickel sulfide, composition and purity. Figure 9 shows the X-ray diffraction (XRD) pattern of NiS/Graphene. All the characteristic diffraction peaks are assigned to different planes of NiS crystalline structure, in which the peak at  $30^\circ$  belongs to (100) plane, peak at  $35^\circ$  belongs to (101) plane, peak at  $46^\circ$  belongs to (102) plane and peak at  $53^\circ$  belongs to (110) plane of NiS.<sup>44</sup> The result indicates that after sulfurization, the only metal sulfide in the composite is NiS without other impurity.

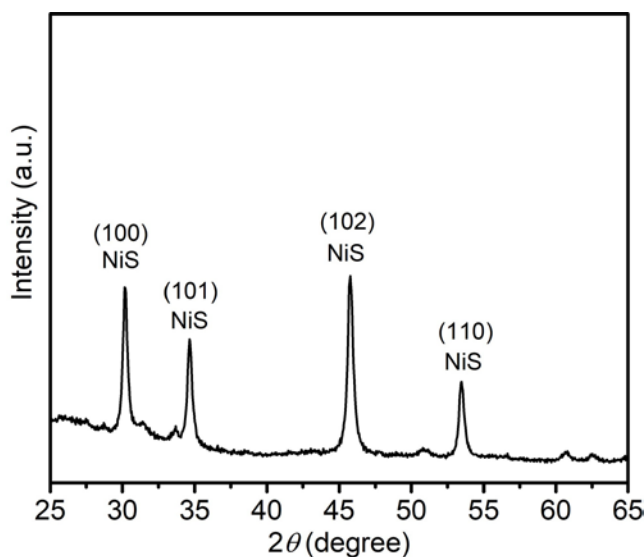


Figure 9. X-ray diffraction (XRD) pattern of the composite after sulfurization, indicating the formation of NiS from Ni ion.

### 3.3 Thermal analysis for composite composition

In order to precisely convert the carbon-coated Ni/Graphene composite to the NiS/Graphene composite, the sulfurization temperature should be determined at first. Thus, a mixture of carbon-coated Ni/Graphene composite and thiourea is prepared to conduct thermal gravimetric analysis (TGA) to determine sulfurizing temperature, as is shown in Figure 10. Also, to keep consistent, the mass ratio in the mixture is 3:1, the same condition as sulfurization process. The condition of this analysis was raising the temperature to 500 °C with a ramp-rate of 10 °C min<sup>-1</sup> under N<sub>2</sub> atmosphere. In Figure 10, there was a weight loss from 120 to 200 °C owing to the decomposition of thiourea:



The decomposition of thiourea is also fit to the first peak in derivation weight percentage curve. There was a second peak in the red curve at 420 °C, indicating another reaction happened. This reaction should belong to the reaction of H<sub>2</sub>S formed by the decomposition of thiourea and the Ni ion to form NiS:  $\text{H}_2\text{S} + \text{Ni}^{2+} \rightarrow \text{NiS} + 2\text{H}^+$ .

Figure 11 shows the TGA result of NiS/Graphene composite. The condition was raising temperature to 600 °C with a ramp-rate of 10 °C min<sup>-1</sup> under air atmosphere. There was a weight loss in the curve, which was belonged to carbon content converting to carbon dioxide (CO<sub>2</sub>) in air, indicating the carbon in the composite is 22 %. The carbon in the composite is consist of the carbon coating derived from decomposition of trimesic acid organic ligand during carbonization process and the graphene derived from graphene oxide (GO). In other words, the TGA result suggests that the NiS content in the composite is 78 %.

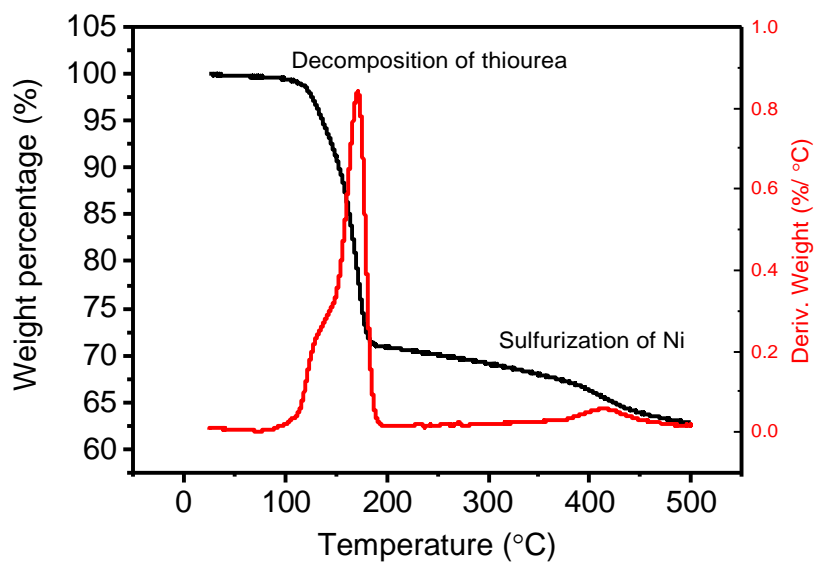


Figure 10. Thermal gravimetric analysis (TGA) of carbon-coated Ni/Graphene composite and thiourea mixture. (N<sub>2</sub>; temperature: raised to 500 °C; ramp-rate: 10 °C min<sup>-1</sup>)

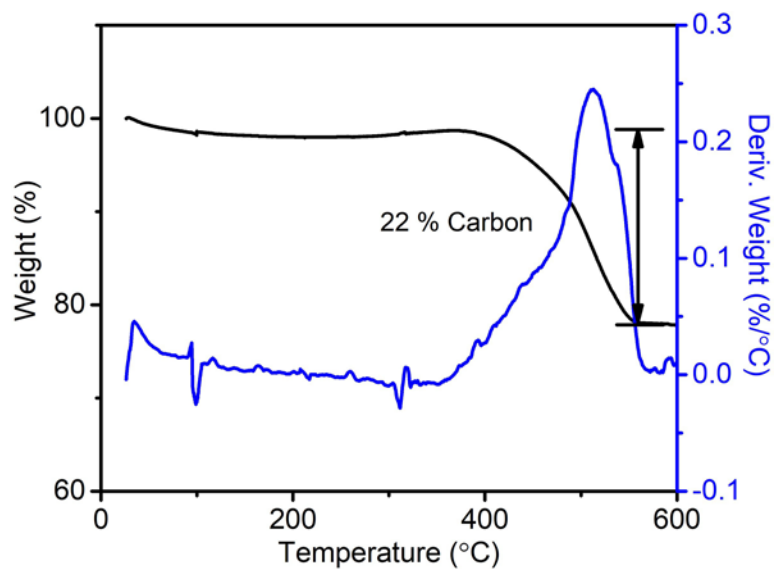


Figure 11. Thermal gravimetric analysis of NiS/Graphene composite. (Air; temperature: raised to 600 °C; raising ramp-rate: 10 °C min<sup>-1</sup>)

### 34 Characterization of graphene in the composite

As is shown in Figure 12, Raman spectrum was conducted to characterized graphene in the NiS/Graphene composite. For Ni-MOF/Graphene composite,  $I_D/I_G = 1.071$ , while the ratio for NiS/Graphene composite reduced to 0.991. It indicates that in NiS/Graphene, the ratio of G band (refers to  $sp^2$  hybridized orbital) increased. Also, the 2D band ratio (refers to layer number in graphene sheets) in NiS/Graphene composite is higher than that in Ni-MOF/Graphene precursor. Both results indicate that after carbonization and sulfurization, the character of graphene increases, which is consistent with the SEM images (Figure 8 b-d).

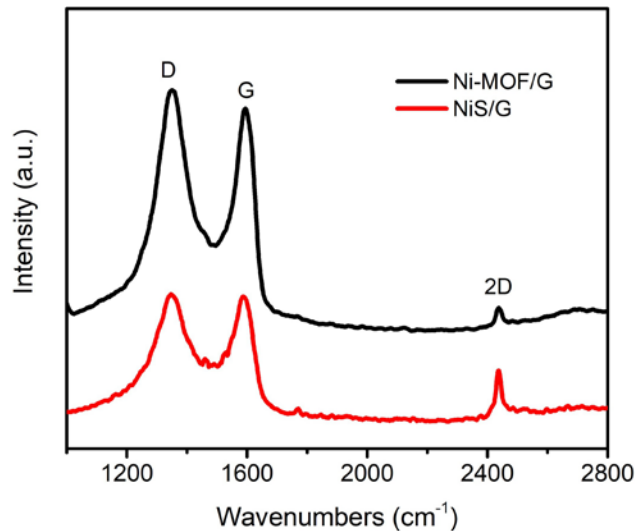


Figure 12. Raman spectrum of Ni-MOF/Graphene and NiS/Graphene composite.

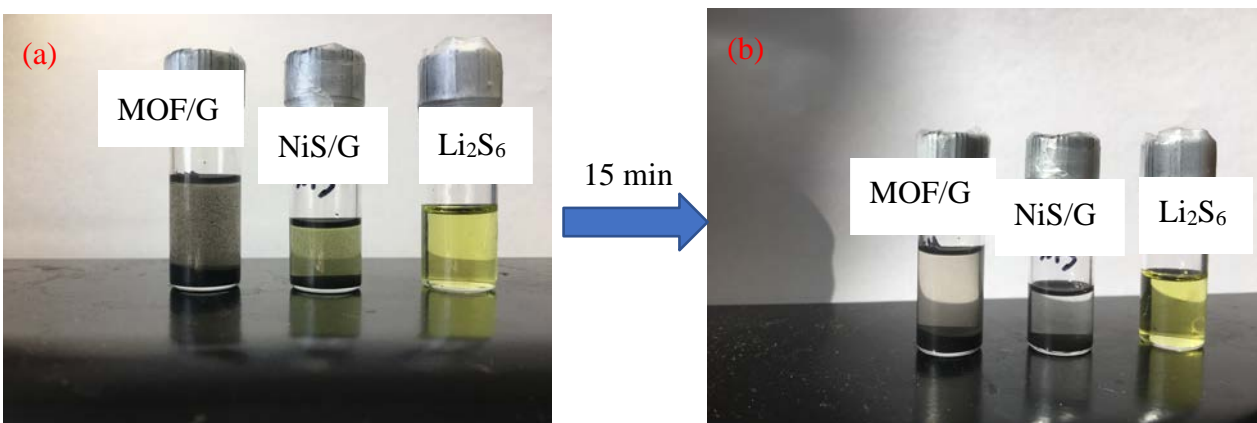
### 35 Lithium polysulfide adsorption test

Nickel sulfide (NiS) was synthesized in the composite owing to metal sulfide's intrinsic property of affinity to lithium polysulfide, and we believe NiS could help to

mitigate the shuttle effect in our Li-S cells. Thus, a lithium polysulfide adsorption test was then conducted to examine the absorbing capability of NiS/Graphene composite. The lithium polysulfide solution ( $\text{Li}_2\text{S}_6$ ) was prepared by dissolving lithium metal and sulfur in 1,3-Dioxolane (DOL) and 1,2-Dimethoxyethane (DME) solution (volume ratio = 1:1) and stirring for 2 days. The color of  $\text{Li}_2\text{S}_6$  solution is yellow.

First, same amount of a low concentration of  $\text{Li}_2\text{S}_6$  was added to 5 mg of Ni-MOF/Graphene and 5 mg NiS/Graphene to conduct comparison test (Figure 13a). After 15 minutes of absorption, both Ni-MOF/Graphene solution and NiS/Graphene solution turned from yellow to colorless (Figure 13b), indicating that both Ni-MOF/Graphene precursor and NiS/Graphene composite has a good absorption ability for lithium polysulfide.

Then, a further higher concentration of  $\text{Li}_2\text{S}_6$  (color was deeper) was prepared and used same condition to test absorption capability (Figure 13c). After 30-minute-absorption, Ni-MOF/Graphene solution remained yellow, however, NiS/Graphene solution turned to colorless again (Figure 13d). This result confirms that NiS/Graphene composite has a higher absorption ability than Ni-MOF/Graphene precursor, and it has a great affinity to lithium polysulfide, which could help to mitigate shuttle effect in cells.



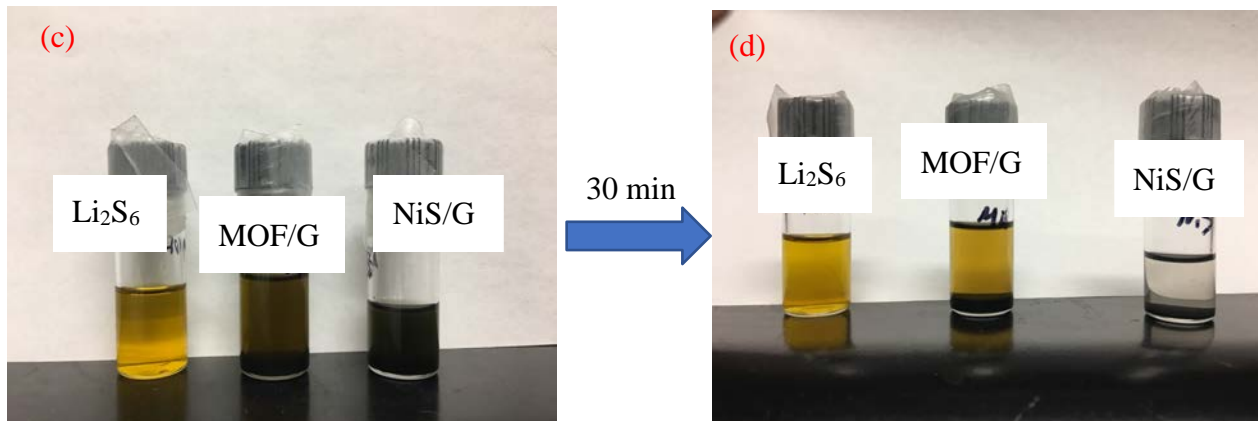


Figure 13. Lithium polysulfide ( $\text{Li}_2\text{S}_6$ ) absorption test. (a) drop a low concentration of  $\text{Li}_2\text{S}_6$  solution in Ni-MOF/Graphene precursor and NiS/Graphene composite. (b) change of MOF/Graphene precursor and NiS/Graphene composite after 15 min absorption of  $\text{Li}_2\text{S}_6$ . (c) drop a high concentration of  $\text{Li}_2\text{S}_6$  solution in Ni-MOF/Graphene precursor and NiS/Graphene composite. (d) change of MOF/Graphene precursor and NiS/Graphene composite after 30 min absorption of  $\text{Li}_2\text{S}_6$ .

### 3.6 Electrochemical performances

#### 3.6.1 Cyclic voltammetry (CV)

After characterization, the NiS/Graphene was used as active material in a lithium-sulfur battery. Also, element sulfur was added in active material as sulfur source with a ratio of sulfur : NiS/Graphene = 7 : 3. Then, the cyclic voltammetry test was conducted at a voltage window of 1.7-2.8 V with a scan rate of  $0.2 \text{ mV s}^{-1}$ , and the profile is shown in Figure 14.

At the first two cycles, there was only one anodic peak at 2.5 V and one cathodic peak at 2.1 V. The reason is that at first two cycles, the Li-S was during the activation process, the cell was not such stable that the profile was a bit different from normal Li-S cells.<sup>45</sup> After activation, from 3<sup>rd</sup> cycle to 6<sup>th</sup> cycle, there appeared two anodic peaks at 2.4 V and 2.5 V, and two cathodic peaks at 2.1V and 1.9 V. The cathodic peaks indicates the conversion from element sulfur to long-chain polysulfide at 2.1 V and further reduced to short-chain polysulfide at 1.9 V. However, the peak at 1.9 V became a slope when further reducing voltage. According to Wang et al.<sup>46</sup>, when using NiS as cathode active material for lithium ion battery, between 1.4-1.8 V, there happens a reaction:  $2\text{Li} + \text{NiS} \rightarrow \text{Li}_2\text{S} + \text{Ni}$ . That may cause the peak at 1.9 V of Li-S cell became a slope when voltage decreased. Figure 15 shows 1<sup>st</sup> cycle charge/discharge profile of the cell at 0.15 C (1 C = 1675 mA g<sup>-1</sup>), the two plateaus at 2.3 V and 2.1 V in the discharge curve correspond to the cathodic peaks in the CV curve.

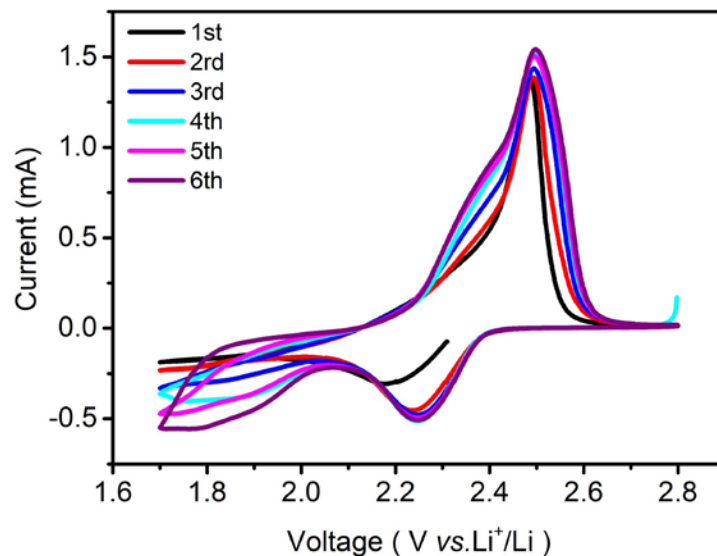


Figure 14. Cyclic voltammetry (CV) curve of Li-S cell test at voltage window of 1.7-2.8 V with a scan rate of 0.2 mV s<sup>-1</sup>.

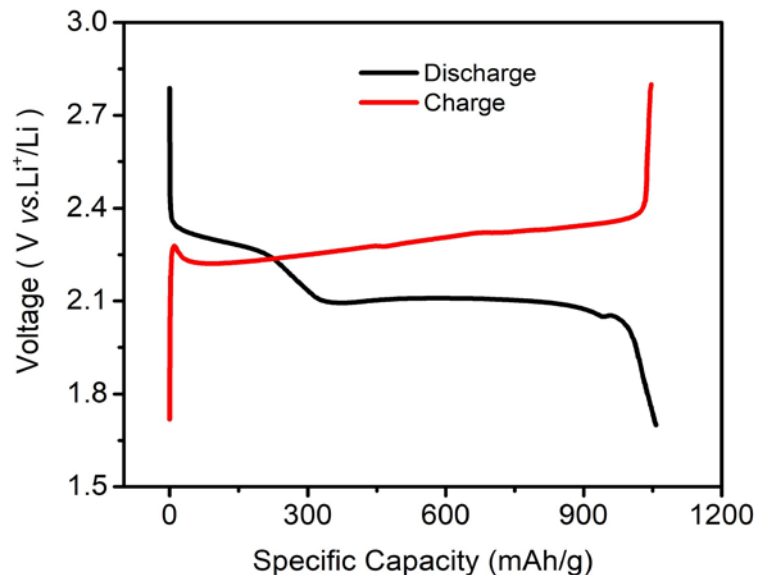


Figure 15. Charge/discharge (specific capacity vs. voltage) profile for 1<sup>st</sup> cycle at current density of 0.15 C (1 C = 1675 mA g<sup>-1</sup>).

### 3.6.2 Galvanostatic charge/discharge test

After conducting cyclic voltammetry test to investigate mechanism, galvanostatic charge and discharge test was then carried out. As is shown in Figure 16, the Li-S cell was tested at 0.05 C, 0.15 C and 0.75 C separately. At current density of 0.05 C, a discharge capacity of 1398 mA h g<sup>-1</sup> was delivered at 1<sup>st</sup> cycle with a further reversible capacity of 1366 mA h g<sup>-1</sup>. The 1<sup>st</sup> cycle reached a coulombic efficiency of 97.7 %, which is reasonably high for cathode material. A 1<sup>st</sup> cycle discharge/charge capacity of 1057 mA h g<sup>-1</sup> and 1047 mA h g<sup>-1</sup> was obtained at 0.15 C with a higher first cycle coulombic efficiency of 99 %. After tested for 100 cycles at 0.15 C, the reversible capacity reached at 799 mA h g<sup>-1</sup> with the retention of 76.3 % and 0.24 % decay per cycle.

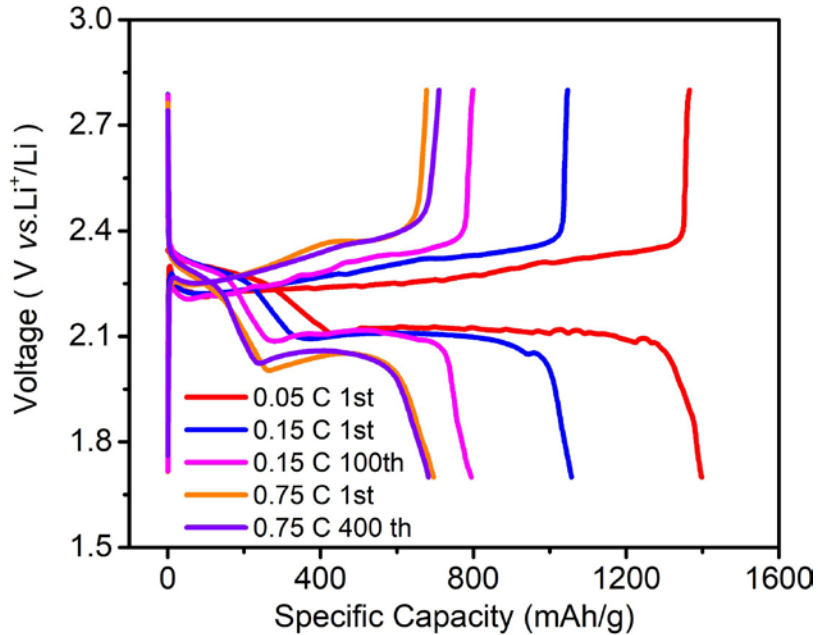


Figure 16. Galvanostatic charge/discharge profile (voltage vs. specific capacity) of 1<sup>st</sup> cycle at current density of 0.05 C, 1<sup>st</sup> and 100<sup>th</sup> cycle at 0.15 C, 1<sup>st</sup> and 400<sup>th</sup> cycle at 0.75 C.

### 3.6.3 Rate capability

C-rate performance was then tested by running the cell at different current density from 0.05 C to 3 C, as shown in Figure 17. At 0.05 C, the cell had a fast capacity decay after first cycle because the cell is in activation process, and after first cycle, solid electrolyte interface (SEI) layer was formed, which made the cell unstable. At current density of 0.15 C, 0.75 C and 1.5 C, the average capacity could reach to 960 mA h g<sup>-1</sup>, 804 mA h g<sup>-1</sup> and 709 mA h g<sup>-1</sup>. Even at a much higher current density of 3 C, an average reversible capacity of 609 mA h g<sup>-1</sup> is obtained. In addition, from 0.15 C to 3 C, the cell was tested for 10 cycles at each current density, the capacity was relatively stable with low decay of 0.53 %, 0.11 %, 0.36 %, and 0.42 % per cycle respectively. Furthermore, the

current density was finally returned back to a low one of 0.1 C to test the stability. The average capacity reached to 897 mA h g<sup>-1</sup>, which further confirms the Li-S cell has a pretty good c-rate performance and stability.

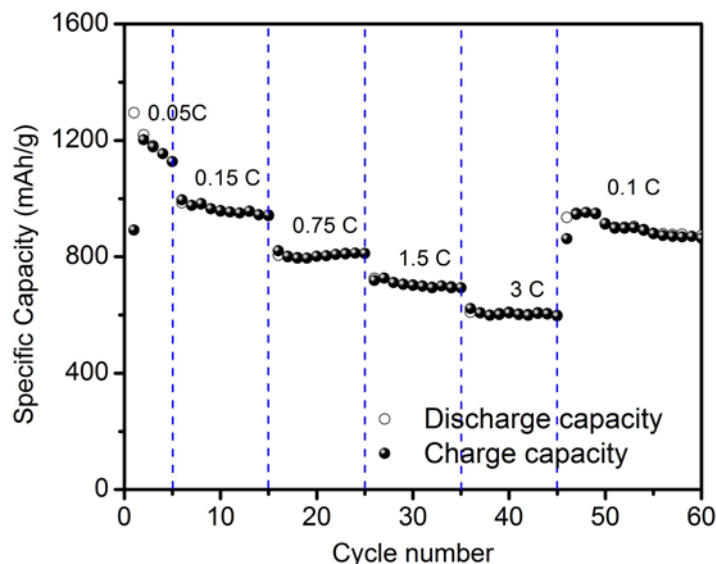


Figure 17. Rate capability of Li-S cells tested at different current density from 0.05 C to 3 C.

### 3.6.4 Long cycle performance

Eventually, a long cycle performance was tested to further investigate the stability of the Li-S cell and Figure 18 shows the result. At first, a low current density of 0.05 C was used to activate the cell, which led to a rapid capacity decay at first several cycles. Then, a little higher current density of 0.15 C was used to make the cell stable faster. After 50 cycles, the cell tended to be stable as the capacity decay decreased a lot. Then, the long cycle performance was tested at 0.75 C. The first cycle obtained a discharge capacity of 696 mA h g<sup>-1</sup> and still reached to 682 mA h g<sup>-1</sup> with a high retention of 98 %. As for the

coulombic efficiency, the average one could reach to 100 % in 0.05 C, 0.15 C and 0.75 C. These two results both indicate that the stability of our Li-S cell is very good, which means the shuttle effect is indeed mitigated by the S/NiS/Graphene electrode we prepare.

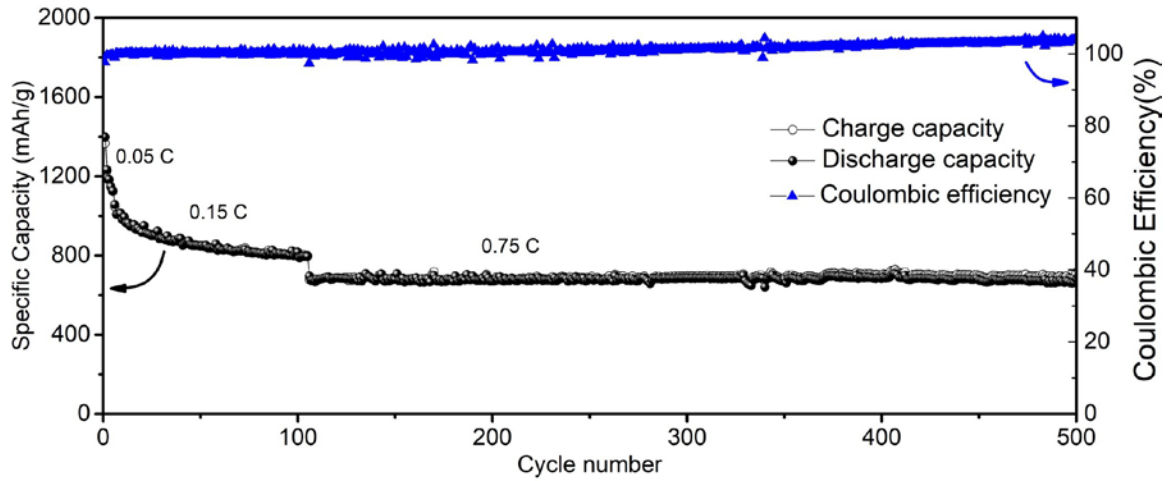


Figure 18. Long cycle performance (capacity/coulombic efficiency vs. cycle) of Li-S cell tested at 0.75 C. (0.05 C and 0.15 C was used for activation).

## CHAPTER IV

### CONCLUSIONS

In this project, a novel nickel sulfide/Graphene composite was synthesized, which was derived from metal organic framework (MOF) precursor. The composite combined the advantages from MOF, metal sulfide and graphene, so that the composite could not only provide good adsorption capability of lithium polysulfide, but also prevent nanoparticles from aggregating with each other. Then lithium-sulfur battery showed improved electrochemical performances when cooperating NiS/Graphene composite with element sulfur as active material in cathode. The cell reached a reversible capacity of  $1366 \text{ mA h g}^{-1}$  at  $0.05 \text{ C}$  ( $1 \text{ C} = 1675 \text{ mA g}^{-1}$ ), and a high reversible capacity of  $609 \text{ mA h g}^{-1}$  at a high current density of  $3 \text{ C}$ . In addition, a retention of  $98 \%$  was obtained after tested for 400 cycles at  $0.75 \text{ C}$  and average coulombic efficiency reached  $100 \%$  at each current density. These results confirm that our NiS/Graphene composite could help to mitigate shuttle effect of lithium polysulfide and improve the whole performances of our Li-S cell. This unique material may could provide a new pathway for cathode material of lithium-sulfur battery in the future.

## REFERENCES

1. Rosenman, A., Markevich, E., Salitra, G., Aurbach, D., Garsuch, A., & Chesneau, F. (2015). Review on Li-sulfur battery systems: an Integral perspective. *Advanced Energy Materials*, 5(16).
2. Yang, Y., Zheng, G., & Cui, Y. (2013). Nanostructured sulfur cathodes. *Chemical Society Reviews*, 42(7), 3018–3032.
3. Zou, F., Chen, Y.-M., Liu, K., Yu, Z., Liang, W., Bhaway, S. M., ... Zhu, Y. (2015). Metal organic frameworks derived hierarchical hollow NiO/Ni/graphene composites for lithium and sodium storage. *ACS Nano*, 10(1), 377–386.
4. Erickson, E. M., Ghanty, C., & Aurbach, D. (2014). New horizons for conventional lithium ion battery technology. *The Journal of Physical Chemistry Letters*, 5(19), 3313–3324.
5. Lu, L., Han, X., Li, J., Hua, J., & Ouyang, M. (2013). A review on the key issues for lithium-ion battery management in electric vehicles. *Journal of Power Sources*, 226, 272–288.
6. Sun, F., Hu, X., Zou, Y., & Li, S. (2011). Adaptive unscented Kalman filtering for state of charge estimation of a lithium-ion battery for electric vehicles. *Energy*, 36(5), 3531–3540.

7. Jung, Y. S., Cavanagh, A. S., Dillon, A. C., Groner, M. D., George, S. M., & Lee, S.-H. (2010). Enhanced stability of LiCoO<sub>2</sub> cathodes in lithium-ion batteries using surface modification by atomic layer deposition. *Journal of The Electrochemical Society*, 157(1), A75–A81
8. Yuan, L.-X., Wang, Z.-H., Zhang, W.-X., Hu, X.-L., Chen, J.-T., Huang, Y.-H., & Goodenough, J. B. (2011). Development and challenges of LiFePO<sub>4</sub> cathode material for lithium-ion batteries. *Energy & Environmental Science*, 4(2), 269–284.
9. Liu, X., Huang, J., Zhang, Q., & Mai, L. (2017). Nanostructured metal oxides and sulfides for lithium–sulfur batteries. *Advanced Materials*.
10. Manthiram, A., Chung, S., & Zu, C. (2015). Lithium–sulfur batteries: progress and prospects. *Advanced Materials*, 27(12), 1980–2006.
11. Qie, L., Zu, C., & Manthiram, A. (2016). A High Energy Lithium-Sulfur Battery with Ultrahigh-Loading Lithium Polysulfide Cathode and its Failure Mechanism. *Advanced Energy Materials*, 6(7).
12. Zhang, S. S. (2013). Liquid electrolyte lithium/sulfur battery: fundamental chemistry, problems, and solutions. *Journal of Power Sources*, 231, 153–162.
13. Zhang, S. S. (2013). Liquid electrolyte lithium/sulfur battery: fundamental chemistry, problems, and solutions. *Journal of Power Sources*, 231, 153–162.
14. Wang, D.-W., Zeng, Q., Zhou, G., Yin, L., Li, F., Cheng, H.-M., ... Lu, G. Q. M. (2013). Carbon–sulfur composites for Li–S batteries: status and prospects. *Journal of Materials Chemistry A*, 1(33), 9382–9394.

15. Yin, Y., Xin, S., Guo, Y., & Wan, L. (2013). Lithium–sulfur batteries: electrochemistry, materials, and prospects. *Angewandte Chemie International Edition*, 52(50), 13186–13200.
16. Wild, M., O'Neill, L., Zhang, T., Purkayastha, R., Minton, G., Marinescu, M., & Offer, G. J. (2015). Lithium sulfur batteries, a mechanistic review. *Energy & Environmental Science*, 8(12), 3477–3494.
17. Seh, Z. W., Li, W., Cha, J. J., Zheng, G., Yang, Y., McDowell, M. T., ... Cui, Y. (2013). Sulphur–TiO<sub>2</sub> yolk–shell nanoarchitecture with internal void space for long-cycle lithium–sulphur batteries. *Nature Communications*, 4, 1331.
18. Wang, Q., Jin, J., Wu, X., Ma, G., Yang, J., & Wen, Z. (2014). A shuttle effect free lithium sulfur battery based on a hybrid electrolyte. *Physical Chemistry Chemical Physics*, 16(39), 21225–21229.
19. Xiao, Z., Yang, Z., Wang, L., Nie, H., Zhong, M., Lai, Q., ... Huang, S. (2015). A lightweight TiO<sub>2</sub>/graphene interlayer, applied as a highly effective polysulfide absorbent for fast, long-life lithium–sulfur batteries. *Advanced Materials*, 27(18), 2891–2898.
20. Sun, Z., Zhang, J., Yin, L., Hu, G., Fang, R., Cheng, H.-M., & Li, F. (2017). Conductive porous vanadium nitride/graphene composite as chemical anchor of polysulfides for lithium-sulfur batteries. *Nature Communications*, 8, 14627.
21. Dai, C., Lim, J., Wang, M., Hu, L., Chen, Y., Chen, Z., ... Li, Y. (2018). Honeycomb-Like Spherical Cathode Host Constructed from Hollow Metallic and Polar Co<sub>9</sub>S<sub>8</sub> Tubules for Advanced Lithium–Sulfur Batteries. *Advanced Functional Materials*.

22. Liu, Y., Wang, W., Wang, A., Jin, Z., Zhao, H., & Yang, Y. (2017). A polysulfide reduction accelerator–NiS<sub>2</sub>-modified sulfurized polyacrylonitrile as a high performance cathode material for lithium–sulfur batteries. *Journal of Materials Chemistry A*, 5(42), 22120–22124.
23. Douglas, A., Carter, R., Oakes, L., Share, K., Cohn, A. P., & Pint, C.L. (2015). Ultrafine iron pyrite (FeS<sub>2</sub>) nanocrystals improve sodium–sulfur and lithium–sulfur conversion reactions for efficient batteries. *ACS Nano*, 9(11), 11156–11165.
24. Garsuch, A., Herzog, S., Montag, L., Krebs, A., & Leitner, K. (2012). Performance of Blended TiS<sub>2</sub>/Sulfur/Carbon Cathodes in Lithium-Sulfur Cells. *ECS Electrochemistry Letters*, 1(1), A24–A26.
25. Rui, X., Tan, H., & Yan, Q. (2014). Nanostructured metal sulfides for energy storage. *Nanoscale*, 6(17), 9889–9924.
26. Lv, H., Qiu, S., Lu, G., Fu, Y., Li, X., Hu, C., & Liu, J. (2015). Nanostructured antimony/carbon composite fibers as anode material for lithium-ion battery. *Electrochimica Acta*, 151, 214–221.
27. Zhao, X., Sánchez, B. M., Dobson, P. J., & Grant, P. S. (2011). The role of nanomaterials in redox-based supercapacitors for next generation energy storage devices. *Nanoscale*, 3(3), 839–855.
28. Bruce, P. G., Scrosati, B., & Tarascon, J. (2008). Nanomaterials for rechargeable lithium batteries. *Angewandte Chemie International Edition*, 47(16), 2930–2946.
29. Rui, X., Sim, D., Xu, C., Liu, W., Tan, H., Wong, K., ... Yan, Q. (2012). One-pot synthesis of carbon-coated VO<sub>2</sub> (B) nanobelts for high-rate lithium storage. *RSC Advances*, 2(3), 1174–1180.

30. Wang, Y., & Cao, G. (2008). Developments in nanostructured cathode materials for high-performance lithium-ion batteries. *Advanced Materials*, 20(12), 2251–2269.
31. Zou, F., Hu, X., Li, Z., Qie, L., Hu, C., Zeng, R., Jiang, Y., Huang, Y. (2014). Metal organic frameworks-derived Co<sub>3</sub>O<sub>4</sub> hollow dodecahedrons with controllable interiors as outstanding anodes for Li storage. *Journal of Materials Chemistry A*, 2(31), 12194–12200.
32. Stock, N., & Biswas, S. (2011). Synthesis of metal-organic frameworks (MOFs): routes to various MOF topologies, morphologies, and composites. *Chemical Reviews*, 112(2), 933–969.
33. Liu, X., Zou, F., Liu, K., Qiang, Z., Taubert, C. J., Ustriyana, P., ... Zhu, Y. (2017). A binary metal organic framework derived hierarchical hollow Ni<sub>3</sub>S<sub>2</sub>/Co<sub>9</sub>S<sub>8</sub>/N-doped carbon composite with superior sodium storage performance. *Journal of Materials Chemistry A*, 5(23), 11781–11787.
34. Chen, Y.-M., Liang, W., Li, S., Zou, F., Bhaway, S. M., Qiang, Z., ... Zhu, Y. (2016). A nitrogen doped carbonized metal–organic framework for high stability room temperature sodium–sulfur batteries. *Journal of Materials Chemistry A*, 4(32), 12471–12478.
35. Shao, J., Wan, Z., Liu, H., Zheng, H., Gao, T., Shen, M., ... Zheng, H. (2014). Metal organic frameworks-derived Co<sub>3</sub>O<sub>4</sub> hollow dodecahedrons with controllable interiors as outstanding anodes for Li storage. *Journal of Materials Chemistry A*, 2(31), 12194–12200.

36. Sharmin, E., & Zafar, F. (2016). Introductory Chapter: Metal Organic Frameworks (MOFs). In *Metal-Organic Frameworks*. InTech.
37. Ye, C., Zhang, L., Guo, C., Li, D., Vasileff, A., Wang, H., & Qiao, S. (2017). A 3D Hybrid of Chemically Coupled Nickel Sulfide and Hollow Carbon Spheres for High Performance Lithium–Sulfur Batteries. *Advanced Functional Materials*, 27(33).
38. Liang, C., Dudney, N. J., & Howe, J. Y. (2009). Hierarchically structured sulfur/carbon nanocomposite material for high-energy lithium battery. *Chemistry of Materials*, 21(19), 4724–4730.
39. Lei, T., Chen, W., Huang, J., Yan, C., Sun, H., Wang, C., ... Xiong, J. (2017). Multi-Functional Layered WS<sub>2</sub> Nanosheets for Enhancing the Performance of Lithium–Sulfur Batteries. *Advanced Energy Materials*, 7(4).
40. Zhang, S., Yu, X., Yu, H., Chen, Y., Gao, P., Li, C., & Zhu, C. (2014). Growth of ultrathin MoS<sub>2</sub> nanosheets with expanded spacing of (002) plane on carbon nanotubes for high-performance sodium-ion battery anodes. *ACS Applied Materials & Interfaces*, 6(24), 21880–21885.
41. Ji, L., Rao, M., Zheng, H., Zhang, L., Li, Y., Duan, W., ... Zhang, Y. (2011). Graphene oxide as a sulfur immobilizer in high performance lithium/sulfur cells. *Journal of the American Chemical Society*, 133(46), 18522–18525.
42. Xia, F., Kwon, S., Lee, W. W., Liu, Z., Kim, S., Song, T., ... Park, W. Il. (2015). Graphene as an interfacial layer for improving cycling performance of Si nanowires in lithium-ion batteries. *Nano Letters*, 15(10), 6658–6664.

43. Zhou, G., Yin, L.-C., Wang, D.-W., Li, L., Pei, S., Gentle, I. R., ... Cheng, H.-M. (2013). Fibrous hybrid of graphene and sulfur nanocrystals for high-performance lithium–sulfur batteries. *Acs Nano*, 7(6), 5367–5375.
44. Kristl, M., Dojer, B., Gyergyek, S., & Kristl, J. (2017). Synthesis of nickel and cobalt sulfide nanoparticles using a low cost sonochemical method. *Heliyon*, 3(3), e00273.
45. Chen, S., Dai, F., Gordin, M. L., & Wang, D. (2013). Exceptional electrochemical performance of rechargeable Li–S batteries with a polysulfide-containing electrolyte. *Rsc Advances*, 3(11), 3540–3543.
46. Wang, Z., Li, X., Yang, Y., Cui, Y., Pan, H., Wang, Z., ... Qian, G. (2014). Highly dispersed  $\beta$ -NiS nanoparticles in porous carbon matrices by a template metal–organic framework method for lithium-ion cathode. *Journal of Materials Chemistry A*, 2(21), 7912–7916.